matings. Average egg-hatching rate in 64 full-sib matings representing all founder families was 60%, compared to 79% in 48 non-sib crosses within and between populations.

Received 22 September 1997; accepted 4 February 1998.

1. Frankham, R. Conservation genetics. *Annu. Rev. Genet.* **29,** 305–327 (1995).
2. Frankham, R. Inbreeding and extinction: a threshold effect. *Conserv. Biol.* **9,** 792–799 (1995).
3. Charlesworth, D. & Charlesworth, B. Inbreeding depression and its evolutionary consequences. *Annu. Rev. Ecol. Syst.* **18,** 237–268 (1987).
4. Ralls, K., Ballou, J. D. & Templeton, A. Estimates of lethal equivalents and the cost of inbreeding in mammals. *Conserv. Biol.* **2,** 185–193 (1988).
5. Thornhill, N. W. (ed.) *The Natural History of Inbreeding and Outbreeding: Theoretical and Empirical Perspectives* (University of Chicago Press, Chicago, 1993).
6. Falconer, D. S. & Mackay, T. F. C. *Introduction to Quantitative Genetics* 4th edn (Longman, Burnt Mill, Harlow, UK, 1996).
7. Saccheri, I. J., Brakefield, P. M. & Nichols, R. A. Severe inbreeding and rapid fitness rebound in the butterfly *Bicyclus anynana* (Satyridae). *Evolution* **50,** 2000–2013 (1996).
8. Jiménez, J. A., Hughes, K. A., Alaks, G., Graham, L. & Lacy, R. C. An experimental study of inbreeding depression in a natural habitat. *Science* **266,** 271–273 (1994).
9. Newman, D. & Pilson, D. Increased probability of extinction due to decreased effective population size: experimental populations of *Clarkia pulchella*. *Evolution* **51,** 354–362 (1997).
10. Keller, L. F., Arcese, P., Smith, J. N. M., Hochachka, W. M. & Stearns, S. C. Selection against inbred song sparrows during a natural population bottleneck. *Nature* **372,** 356–357 (1994).
11. Madsen, T., Stille, B. & Shine, R. Inbreeding depression in an isolated population of adders *Vipera berus*. *Biol. Conserv.* **75,** 113–118 (1996).
12. Caro, T. M. & Laurenson, M. K. Ecological and genetic factors in conservation: a cautionary tale. *Science* **263,** 485–486 (1994).
13. Caughley, G. Directions in conservation biology. *Anim. Ecol.* **63,** 215–244 (1994).
14. Hanski, I. A. & Gilpin, M. E. (eds) *Metapopulation Biology: Ecology, Genetics, and Evolution* (Academic, San Diego, 1997).
15. Hanski, I., Pakkala, T., Kuussaari, M. & Lei, G. Metapopulation persistence of an endangered butterfly in a fragmented landscape. *Oikos* **72,** 21–28 (1995).
16. Lande, R. Genetics and demography in biological conservation. *Science* **241,** 1455–1460 (1988).
17. Hanski, I., Pöyry, J., Pakkala, T. & Kuussaari, M. Multiple equilibria in metapopulation dynamics. *Nature* **377,** 618–621 (1995).
18. Hanski, I., Moilanen, A., Pakkala, T. & Kuussaari, M. The quantitative incidence function model and persistence of an endangered butterfly metapopulation. *Conserv. Biol.* **10,** 578–590 (1996).
19. Hanski, I. A practical model of metapopulation dynamics. *Anim. Ecol.* **63,** 151–162 (1994).
20. Hanski, I. Metapopulation dynamics: from concepts and observations to predictive models in *Metapopulation Biology: Ecology, Genetics, and Evolution* (eds Hanski, I. A. & Gilpin, M. E.) 69–91 (Academic, San Diego, 1997).
21. Hanski, I., Kuussaari, M. & Nieminen, M. Metapopulation structure and migration in the butterfly *Melitaea cinxia*. *Ecology* **75,** 747–762 (1994).
22. Lei, G. C. & Hanski, I. Metapopulation structure of *Cotesia melitaearum*, a specialist parasitoid of the butterfly, *Melitaea cinxia*. *Oikos* **78,** 91–100 (1997).
23. Kuussaari, M., Nieminen, M. & Hanski, I. An experimental study of migration in the Glanville fritillary butterfly *Melitaea cinxia*. *J. Anim. Ecol.* **65,** 791–801 (1996).
24. Lei, G. C., Vikberg, V., Nieminen, M. & Kuussaari, M. The parasitoid complex attacking Finnish populations of the Glanville fritillary *Melitaea cinxia* (Lep: Nymphalidae), an endangered butterfly. *J. Nat. Hist.* **31,** 635–648 (1997).
25. Wahlberg, N. *One Day in the Life of a Butterfly; a Study of the Glanville Fritillary* Melitaea cinxia (Thesis, Univ. Helsinki, 1995).
26. Hedrick, P. W. Purging inbreeding depression and the probability of extinction: full-sib mating. *Heredity* **73,** 363–372 (1994).
27. Lynch, M., Conery, J. & Bürger, R. Mutation accumulation and the extinction of small populations. *Am. Nat.* **146,** 489–518 (1995).

Acknowledgements. We thank K. Higgins, L. Keller, R. Lande, M. Lynch, A. Moilanen, R. Nichols, S. van Nouhuys, M. Singer and C. Thomas for their helpful comments on the manuscript.

Correspondence and requests for materials should be addressed to I.S. (e-mail: ilik.saccheri@helsinki.fi).

Cerebellar complex spikes encode both destinations and errors in arm movements

Shigeru Kitazawa*†, Tatsuya Kimura* & Ping-Bo Yin§

** Information Science Division, Electrotechnical Laboratory,*
† PRESTO and § CREST, Japan Science and Technology Corporation, 1-1-4 Umezono, Tsukuba 305-8568, Japan

Purkinje cells of the cerebellum discharge complex spikes, named after the complexity of their waveforms[1], with a frequency of ~1 Hz during arm movements[1–13]. Despite the low frequency of firing, complex spikes have been proposed to contribute to the initiation of arm movements[2,7–10] or to the gradual improvement of motor skills[2,4–6,14–16]. Here we recorded the activity of Purkinje cells from the hemisphere of cerebellar lobules IV–VI while trained monkeys made short-lasting reaching movements (of ~200 milliseconds in duration) to touch a visual target that appeared at a random location on a tangent screen. We examined the relationship between complex-spike discharges and the absolute touch position, and between complex-spike discharges and relative errors in touching the screen. We used information theory to show that the complex spikes occurring at the beginning of the reach movement encode the absolute destination of the reach, and the complex spikes occurring at the end of the short-lasting movements encode the relative errors. Thus, complex spikes convey multiple types of information, consistent with the idea that they contribute both to the generation of movements and to the gradual, long-term improvement of these movements.

Two macaque monkeys were trained to make rapid reaching movements toward a visual target that appeared on a tangent screen, located 200 mm from the eyes, from a button positioned 200 mm below the eyes in the mid-sagittal plane. A trial began when the monkey pressed the button (Start, Fig. 1); a target then appeared (Target, Fig. 1) at a random place in a square target zone (50 × 50 mm, or 80 × 80 mm) on the screen. The monkey had to release the button (Release, Fig. 1) within 240 ms of the appearance of the target and touch the screen within 300 ms of releasing the button (Touch, Fig. 1). The monkey's view of its hand and the target was blocked at the release of the button by liquid-crystal shutters in front of the eyes (Release, Fig. 1). The shutters opened again when the screen was touched (Open, Fig. 1), allowing the monkey to see the target and the final position of its hand for 300 ms. The monkey had to hold the final position of its hand for 900 ms until given a reward (Reward, Fig. 1); the size of the reward was in inverse proportion to the magnitude of the error to encourage accurate reaching.

Figure 2 shows a raster plot (Fig. 2a) and the average discharge frequencies (Fig. 2b) of a Purkinje cell from lobule V. Stable simple spikes and complex spikes were recorded from this Purkinje cell during 1,381 trials. The average discharge frequency of simple spikes, (Fig. 2b) decreased to 40 Hz during the movement, and then sharply increased to 170 Hz at the end of the movement (Touch, time zero). In contrast, complex spikes generally occurred only once during each trial (black dots, Fig. 2a) and the average discharge frequency was less sharply altered during the movement (Fig. 2b). To test whether the sporadic complex-spike discharges of this Purkinje cell ever encode absolute destination of the reaching movement or relative errors, we set three time windows (shown with crossed, diagonal or horizontal lines in Fig. 2b).

During the first time window in the first half of the movement (crosshatched area in Fig. 2b), complex-spike discharges occurred in 133 of the 1,381 trials. Figure 3a shows the absolute position of

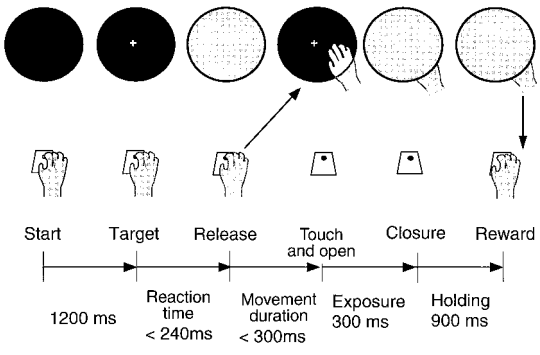

Figure 1 The reaching task. The sequence of events for each trial is shown from left to right. A trial begins when a monkey touches a button. A target beam then appears on the screen. The monkey then releases the button, and touches the target on the screen. At this point, liquid-crystal shutters that were obscuring the monkey's view of its hand are opened for 300 ms, then closed. The monkey holds the position of its hand on the target for 900 ms, and then receives a reward.

touch on the screen in the 1,381 trials (black dots). Results from the 133 trials that showed complex-spike discharges are circled in red. Although the touch positions (black dots) for the 1,381 trials were distributed evenly over the 50×50 mm target zone, the touch positions for the 133 trials that showed complex-spike discharges (red circles) were skewed towards the lower right quadrant of the screen. The number of red circles in each quadrant (counter-clockwise from upper right quadrant: 24, 14, 39, 56) was significantly uneven (χ^2 test, $P < 0.00001$, degrees of freedom d.f. $= 3$, $\chi^2 = 30.3$). Thus, when complex spikes occurred during the initial part of the reach, the monkey was four times more likely to touch the fourth quadrant than the second (56 touches out of 133 versus 14 touches). The predictive information associated with the occurrence of complex spikes (I_{cs}) was quantified as the decrease in entropy in the absolute touch position:

$$I_{cs} = \sum_{i=1}^{4} -(n_i/N)\log_2(n_i/N) - \sum_{i=1}^{4} -(m_i/M)\log_2(m_i/M) \qquad (1)$$

where n_i and m_i denote numbers of black dots and red circles in the ith quadrant, and N and M denote total numbers of black dots and red circles, respectively. If the red circles are confined to a particular quadrant, I_{cs} would yield 2 bits, and if they distribute evenly I_{cs} would yield 0 bits. In Fig. 3a, I_{cs} was 0.2 bits. The information was considered 'significant' when the corresponding χ^2 tests yielded a P value <0.05, as in the present case ($P < 0.00001$).

Errors of reaching relative to the target in the 1,381 trials (black dots in Fig. 3b, c) were distributed in a gaussian manner around the target, as were the errors in the subset of 133 trials with an early complex spike (results not shown). The P value of the χ^2 test was 0.69, indicating that the complex spike conveyed little information ($I_{cs} = 0.01$) about the reaching errors.

During the second time window, just after touching of the screen (shown with oblique lines in Fig. 2b), complex-spike discharges occurred in 92 of the 1,381 trials. The distribution of touch positions in the 92 trials was almost even over the four quadrants (results not shown; $P = 0.76$, $I_{cs} = 0.01$), but relative reaching errors for the 92 trials were distributed preferentially in the upper left quadrant (red circles in Fig. 3b; $P < 0.0001$, $I_{cs} = 0.19$). During the third time window, 120–220 ms after the touch (shown with horizontal lines in Fig. 2b), 88 complex-spike discharges occurred. Relative errors in the 88 trials were distributed preferentially in the left half (red circles in Fig. 3c; $P < 0.0001$, $I_{cs} = 0.18$), but absolute touch positions were evenly distributed (results not shown; $P = 0.71$, $I_{cs} = 0.01$). Thus, the complex-spike discharges during the second and third time windows conveyed significant information about reaching errors.

These three time windows were not chosen arbitrarily. We calculated the information (I_{cs}) on the touch position and on the relative reaching errors by moving a time window of 100 ms along

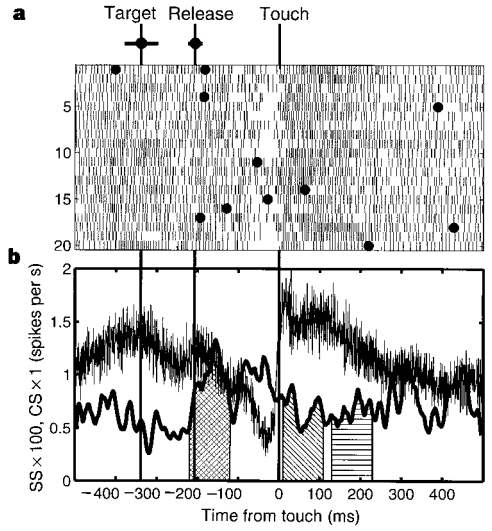

Figure 2 Simple-spike (SS) and complex-spike (CS) activity recorded from a Purkinje cell in lobule V. **a**, A raster plot of SS (vertical bars) and CS (filled dots) activity aligned at the touch (20 trials). **b**, Average discharge frequency (ordinate) of SS activity (thin trace, ×100 Hz) and CS activity (thick trace, ×1 Hz) for 1,381 trials. Bin width is 0.5 ms and the trace for CS activity was smoothened by the moving average method (40-ms window). Mean timing of target appearance and button release is shown by vertical lines, with s.d. (horizontal bars). Three 100-ms time windows are shown with crossed, oblique and horizontal lines, in the lower panel.

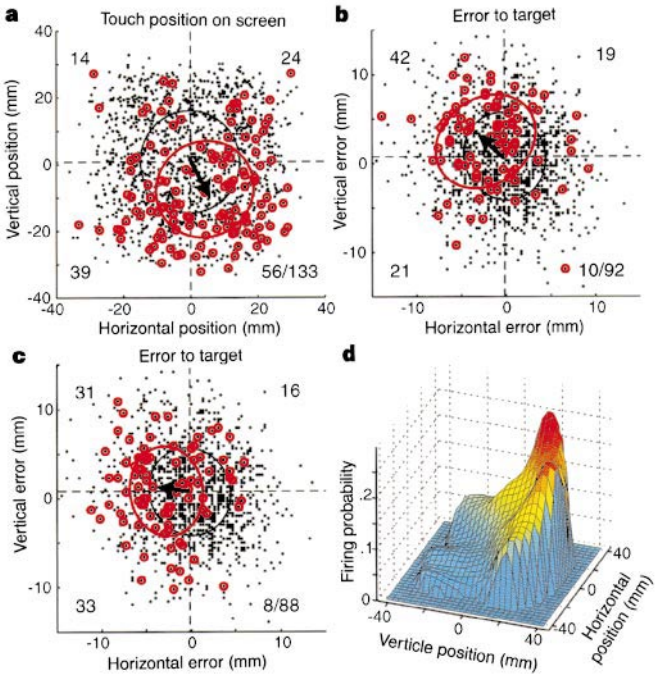

Figure 3 Distribution of touch positions and relative errors. Data are from the same cell used for Fig. 2. **a**, Scatterplots of the touch positions on the screen in all 1,381 trials (black dots), and in the 133 trials (red circles) with complex-spike activity during the first 100-ms window shown in Fig. 2. Horizontal and vertical dashed lines pass through the centre of gravity of the black dots and define the four quadrants. Numbers of red circles in each quadrant are indicated, together with the total number (133) in the fourth quadrant. Black and red ellipses show equidistant points (Mahalanobis distance = 1) from the centre of gravity of the black dots and red circles, respectively. The black arrow connects the centres of gravity of the black dots and the red circles and defines the 'preferred' direction. **b**, **c**, Scatterplots of relative errors to the target (origin) in the 1,381 trials (black dots), and of 92 (**b**) and 88 (**c**) trials (red circles) during which complex-spike activity was seen during the second and the third 100-ms time windows shown in Fig. 2, respectively. **d**, Data shown in **a** transformed into firing probability (z-axis) of complex spikes as a function of touch position. A circular window (radius = 10 mm) was moved with 1-mm steps over the x and y planes in **a**, and the number of red circles within the window was divided by the number of black dots at each position. A median filter (10×10 mm) was also used.

the time axis (abscissa in Fig. 2b) with steps of 10 ms, and calculated the information transmission rate (I_r in bits s^{-1}). I_r can be approximated by the product of I_{cs} and the firing frequency of complex spikes (see Methods). There are three peaks of information (Fig. 4a), corresponding roughly to the three time windows. These three peaks were common in the population of 50 Purkinje cells examined (Fig. 4b). Of these 50 cells, most ($n = 47$) showed changes in simple-spike discharges of >30% of their maximum discharge rates, when aligned at the onset or at the end of the reaching movements. The other three cells, whose simple spikes were not changed, conveyed no significant information concerning either the touch position or the error. Regarding the information encoding in the complex spikes of these 47 cells, 19 (40%) showed a significant first peak (Fig. 4b), 21 (45%) showed a significant second peak, and 19 (40%) showed a significant third peak. Thirty-four cells (72%) contributed to at least one of the three peaks, and eight (17%) contributed to all of the three peaks (Fig. 4a). In the eight cells that had all three peaks, peak 1 was the largest in four cells (Fig. 4a), and peak 3 was the largest in the other four cells.

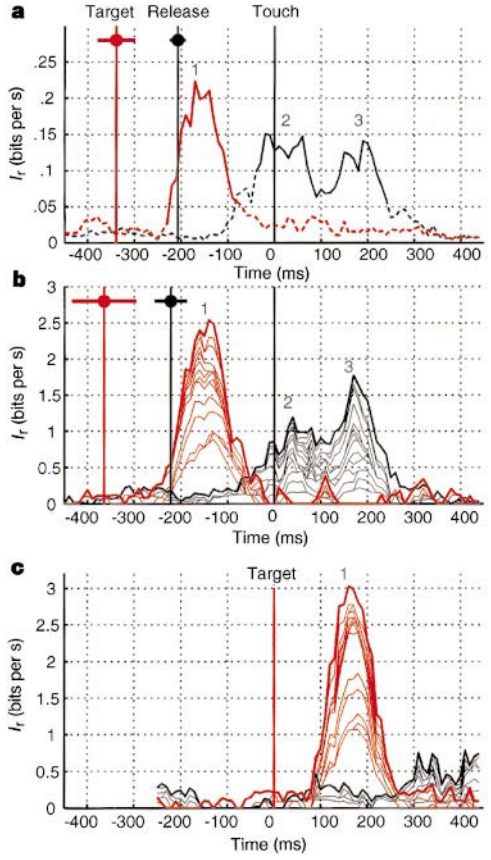

Figure 4 Information transmission rate (I_r) on the touch position (red trace) and the relative error (black trace) encoded by the complex spikes. I_r was calculated using equation (2). **a**, I_r encoded by complex spikes of the same Purkinje cell used for Figs 2, 3. I_r is plotted against the centre of the 100-ms time window that was moved along the time axis (abscissa). Solid and broken traces indicate significant and nonsignificant information, respectively. **b**, **c**, Summation of I_r curves from 50 Purkinje cells aligned on the touch (**b**) and the target appearance (**c**). Nonsignificant information was excluded from the summation. Intervals between the thin lines show the contributions from single cells. This simple summation gives the upper limit of the net information that was encoded by the whole population of cells, as the information from each cell may not be independent. The mean timings for target appearance (red) and release of the button (black) are indicated by vertical lines with horizontal bars (s.d.) in **a**, **b**. Numbers 1–3 in **a**–**c** indicate the peak numbering used in the text.

For the whole population of cells, the preferred directions shown by cells for each of the three peaks of information were distributed almost randomly (results not shown). However, cells that had more than one peak of information showed a consistent pattern of directional preferences. In the 14 cells that had both peaks for relative errors (peaks 2 and 3), the preferred directions for the two peaks usually fell in the same quadrant (in 12 of the 14 cells; difference: 27 ± 34°, mean ± s.d.) and never fell in opposite quadrants. In contrast, the preferred directions for the errors (peak 2 or 3) fell in the quadrant that was opposite to that for the touch position (peak 1) in 7 of 9 cells (for peak 2) and 6 of 10 cells (peak 3), and none of the two pairs ($n = 19$) fell in the same quadrant (difference: 207 ± 40°, mean ± s.d.).

Thus far, we have only partitioned the work space into quadrants and have considered only the encoding of a partial entity of a vector, the direction of movement. By moving a circular window (radius = 10 mm) in 1-mm steps over x and y planes, such as those in Fig. 3d, we were able to map the probability of complex-spike discharge with a higher spatial resolution and thereby show graded information about the magnitude of movements. This analysis showed that the probability of complex-spike discharge increased progressively up to 0.25 as the position shifted in the preferred direction on the touch screen (Fig. 3d). Similar gradations in the probability of discharge were also seen with the relative errors (data not shown). Thus, the complex-spike discharges encode vectors with both magnitude and direction.

Peak 1 became taller when we aligned the summation of I_r curves with the appearance of the target (Fig. 4c, red line), with an onset 80 ms after the appearance of the target, consistent with visual mediation. The earlier peak of information about the relative errors (peak 2, Fig. 4b) cannot have been caused by visual input because vision was blocked by the shutters (Fig. 1) until the screen was touched (time zero), so this peak presumably resulted from somatosensory feedback and/or efference copy. Because of its latency after the touch (when visual error information was first made available), peak 3 (Fig. 4b) also was probably visual in origin and linked to the error at the touch.

Although analysis indicates that complex spikes during peaks 1 and 3 seem to encode different parameters, it is likely that the brain interprets both types of spike as visual motor error, one at the start and the other at the end of the trial, especially as these two peaks tend to show inverse spatial tuning. Only by blocking any view of the hand during reaching were we able to uncover the early visual encoding of touch position (peak 1) and the early non-visual encoding of errors (peak 2), but, in so doing, we excluded any possibility that the complex spikes could signal visual errors during reaching.

What are the roles of the complex spikes that encoded these three peaks of information at different stages of movement? The first peak of information may encode the absolute destination at the beginning of the movement and so might act as a movement-error signal (in spatial coordinates) helping to guide the hand towards the target[2,7–13]. The second and third peaks of information may encode the relative error at the end of the reach; this is too late to affect the ongoing ballistic movement, but might help to improve subsequent movements, that is, to refine motor skills[2,4–6,14–16]. Thus, we suggest that signals for the 'real-time' control and 'learning' of movements[17] are both encoded by complex-spike discharge. □

Methods

Task procedures. We used two monkeys (*Macaca fuscata*, 7.5 kg and 8.5 kg). The monkeys' reaching task is described above and shown in Fig. 1. Eye movements were not controlled during the task. Video pictures showed that the tip of the middle finger touched the screen first in most trials. The animals did not use their palms. The reward was determined by the first position of touch, that is, the position of touch by his middle finger in most trials. The touch screen, liquid-crystal shutters, and reaching task were similar to those used in human experiments[18].

Recording and histological identification of Purkinje-cell locations. After training, a chronic recording chamber was implanted on the skull ipsilateral to the trained arm. Extracellular action potentials of single Purkinje cells were recorded by a glass-coated tungsten microelectrode. Purkinje cells were identified by the presence of spontaneous complex-spike discharge. We recorded as many trials as possible from all Purkinje cells that were encountered, irrespective of their discharge characteristics. The discharges of 161 Purkinje cells were recorded from three hemispheres of the two animals during the reaching task. Simple and complex spikes were discriminated online using a PC-based spike discriminator that applies a principal-component analysis to each spike form[19]. Discriminated trains of simple and complex spikes in each trial were stored on a PC with the timings of the events. In each hemisphere, several penetration tracks were marked by lesions made by passing a direct current (10 μA for 20 s) through the tip of the recording microelectrode. At the end of the recording sessions, the first animal was anaesthetized and perfused with paraformaldehyde. Serial sections of the cerebellum were made. Using the lesions as a reference, recording sites from the first animal ($n = 134$) were all found to be in the intermediate and lateral hemispheres of lobules IV–VI. Data from the second animal are still being recorded but X-ray pictures indicate that the recording locations may be similar to those in the first animal.

Data analysis. Stored data from simple-spike and complex-spike discharges were analysed offline on a workstation (Sun, Ultra 2) using MATLAB. We judged that simple and complex spikes were recorded from isolated Purkinje cells when we confirmed a complete pause in simple spikes for 10 ms after complex-spike onset. Of 161 Purkinje cells, 50 yielded enough data for further analysis in that their simple-spike and complex-spike discharges were recorded for more than 300 trials (33,041 trials in total). Information analysis was applied to each of the 50 cells.

In the analysis, the predictive information available with an occurrence of complex spikes (I_{cs}) was estimated from the decrease in entropy as in equation (1). The amount of information carried by the 'lack' of complex spikes ($I_{\overline{cs}}$) was defined as $I_{\overline{cs}} = \Sigma_{i=1}^{4} - (n_i/N)\log_2(n_i/N) - \Sigma_{i=1}^{4} - ((n_i - m_i)/(N - M)) \times \log_2((n_i - m_i)/(N - N))$, where the notation is the same as in equation (1). The information carried by the complex spikes (I) was defined as:

$$I = p \cdot I_{cs} + (1 - p) \cdot I_{\overline{cs}} \quad (2)$$

where p is the probability of complex-spike occurrence during the time window under consideration. We further defined the information transmission rate, I_r, as $I_r = I/w$, where w denotes the width of the time window. In equation (2), $I_{\overline{cs}}$ was negligibly small, and p is approximated by the product of firing frequency (f) and w as $p \approx fw$. Hence $I_r \approx f \cdot I_{cs}$.

We used time windows of 100, 150 and 200 ms for those cells that were recorded for more than 600 ($n = 26$), 450 ($n = 13$) and 300 ($n = 11$) trials, respectively. The longer time windows were adopted for cells recorded for fewer trials to allow use of the χ^2 test.

The axis that defined the four quadrants was rotated with a step of 10°, and the calculation of the information and P values was repeated nine times. The average of the nine calculations was used for the calculation of I_r, and for the judgement of significance in the χ^2 test.

Received 17 October 1997; accepted 7 January 1998.

1. Thach, W. T. Discharge of Purkinje and cerebelar nuclear neurons during rapidly alternating arm movements in the monkey. *J. Neurophysiol.* **31,** 785–797 (1968).
2. Simpson, J. I., Wylie, D. R. & De Zeeuw, C. I. On climbing fiber signals and their consequence(s). *Behav. Brain Sci.* **19,** 384–398 (1996).
3. Thach, W. T. Discharge of cerebellar neurons related to two maintained postures and two prompt movements. II. Purkinje cell output and input. *J. Neurophysiol.* **33,** 537–547 (1970).
4. Gilbert, P. F. C. & Thach, W. T. Purkinje cell activity during motor learning. *Brain Res.* **128,** 309–328 (1977).
5. Keating, J. G. & Thach, W. T. Nonclock behavior of inferior olive neurons: interspike interval of Purkinje cell complex spike discharge in the awake behaving monkey is random. *J. Neurophysiol.* **73,** 1329–1340 (1995).
6. Thach, W. T. On the specific role of the cerebellum in motor learning and cognition: clues from PET activation and lesion studies in man. *Behav. Brain. Sci.* **19,** 411–431 (1996).
7. Mano, N., Kanazawa, I. & Yamamoto, K. Complex-spike activity of cerebellar P-cells related to wrist tracking movement in monkey. *J. Neurophysiol.* **56,** 137–158 (1986).
8. Mano, N., Kanazawa, I. & Yamamoto, K. Voluntary movements and complex-spike discharges of cerebellar Purkinje cells. *Exp. Brain. Res.* **17,** 265–280 (1989).
9. Bauswein, E., Kolb, F. P., Leimbeck, B. & Rubia, F. J. Simple and complex spike activity of cerebellar Purkinje cells during active and passive movements in the awake monkey. *J. Physiol.* **339,** 379–394 (1983).
10. Wang, J. J., Kim, J. H. & Ebner, T. J. Climbing fiber afferent modulation during a visually guided multijoint arm movement in the monkey. *Brain Res.* **410,** 323–329 (1987).
11. Ojakangas, C. L. & Ebner, T. J. Purkinje cell complex and simple spike changes during a voluntary arm movement learning task in the monkey. *J. Neurophysiol.* **68,** 2222–2236 (1992).
12. Ojakangas, C. L. & Ebner, T. J. Purkinje cell complex spike activity during voluntary motor learning: relationship to kinematics. *J. Neurophysiol.* **72,** 2617–2630 (1994).
13. Fu, Q. G., Mason, C. R., Flament, D., Coltz, J. D. & Ebner, T. J. Movement kinematics encoded in complex spike discharge of primate cerebellar Purkinje cells. *Neuroreport* **8,** 523–529 (1997).
14. Ito, M. *The Cerebellum and Neural Control* (Raven, New York, 1984).
15. Kawato, M. & Gomi, H. A computational model of four regions of the cerebellum based on feedback-error learning. *Biol. Cybern.* **68,** 95–103 (1992).
16. Houk, J. C., Buckingham, J. T. & Barto, A. G. Models of the cerebellum and motor learning. *Behav. Brain Sci.* **19,** 368–383 (1996).
17. Arbib, M. A. Spanning the levels in cerebellar function. *Behav. Brain Sci.* **19,** 434–435 (1996).
18. Kitazawa, S., Kohno, T. & Uka, T. Effects of delayed visual information on the rate and amount of prism adaptation in the human. *J. Neurosci.* **15,** 7644–7652 (1995).
19. Abeles, M. & Goldstein, M. H. Multiple train analysis. *Proc. IEEE* **65,** 762–773 (1977).

Acknowledgements. We thank F. A. Miles and K. Kawano for comments on the manuscript; M. Okui for technical assistance; K. Kurata for useful advice; and S. Yamane and R. Suzuki for encouragement during this study.

Correspondence and requests for materials should be addressed to S.K. (e-mail: kitazawa@etl.go.jp).

Synaptic vesicles retain their identity through the endocytic cycle

Venkatesh N. Murthy & Charles F. Stevens

Howard Hughes Medical Institute and Molecular Neurobiology Laboratory, Salk Institute, 10010 North Torrey Pines Road, La Jolla, California 92037, USA

After fusion of synaptic vesicles with presynaptic membrane and secretion of the contents of the vesicles into the synaptic cleft (a process known as exocytosis), the vesicular membrane is retrieved by endocytosis (internalization) for re-use[1,2]. Several issues regarding endocytosis at central synapses are unresolved, including the location of membrane retrieval (relative to the active zone, where exocytosis occurs), the time course of various endocytic steps, and the recycling path taken by newly endocytosed membranes. The classical model of synaptic-vesicle recycling, proposed by analogy to other cellular endocytic pathways, involves retrieval of the membrane, fusion of the membrane with endosome-like compartments and, finally, budding of new synaptic vesicles from endosomes[1], although the endosomal station may not be obligatory[3]. Here we test the classical model by using the fluorescent membrane dye FM1-43 (refs 4–6) with quantitative fluorescence microscopy. We find that the amount of dye per vesicle taken up by endocytosis equals the amount of dye a vesicle releases on exocytosis; therefore, we conclude that the internalized vesicles do not, as the classical picture suggests, communicate with intermediate endosome-like compartments during the recycling process.

When vesicular membrane internalization occurs in the presence of FM1-43, the dye is trapped inside the endocytosed vesicles[4,5]. Then, when the dye is removed from the external medium, the FM1-43-labelled vesicles can be detected because of their fluorescence. After mild synaptic activity in the presence of FM1-43, the histogram of fluorescence intensity (which reflects the amount of membrane retrieved[4,5]) shows equally spaced peaks[7,8]. Such peaks revealed quantized endocytosis. In the present experiments we aimed to load a few vesicles per synapse with FM1-43 and to measure the decrease in fluorescence when some of these stained vesicles were released. If vesicles maintain their identity through the recycling process, then fluorescence should decrease with release in the same quantal steps as those seen with endocytosis (Fig. 1a, right). If, however, fusion with an endosomal compartment is part of the vesicle-recycling process, the dye should be shared with that compartment and the decrease in fluorescence seen when vesicles are released should occur with smaller steps (Fig. 1a, left).